

Joint Performance Metrics for Integrated Sensing and Communication Systems in Automotive Scenarios

François De Saint Moulin*, Charles Wiame[†], Luc Vandendorpe[‡], Claude Oestges[§]

ICTEAM, UCLouvain - Louvain-la-Neuve, Belgium

*francois.desaintmoulin@uclouvain.be, [†]charles.wiame@uclouvain.be,

[‡]luc.vandendorpe@uclouvain.be, [§]claudio.oestges@uclouvain.be

Abstract—In this paper, multiple metrics are presented in order to jointly evaluate the performance of the radar and communication functions in scenarios involving Dual Function Radar Communication (DFRC) systems using stochastic geometry. These metrics are applied in an automotive scenario involving a two-lane road with vehicles and smart traffic lights, both equipped with DFRC systems. First, the performance achieved with these metrics are validated using Monte-Carlo (MC) simulations. Additionally, optimisation w.r.t. the power of the vehicles and smart traffic lights is performed based on the metrics. Then, the model is extended to include interference cancellation for the radar and/or communication function in all the metrics. Either perfect interference cancellation is applied, or a new model is proposed for imperfect interference cancellation.

Index Terms—DFRC, radar, communication, interference cancellation, automotive scenario, stochastic geometry

I. INTRODUCTION

In recent years, with the spectrum scarcity and the convergence of the carrier frequency ranges used by radar and communication systems, the possibility to operate both functions using the same resources has received an increased attention. Joint radar-communication systems enable to perform both functions simultaneously with a single hardware platform [1]–[3]. Two approaches have been adopted: coexistence and co-design. In the former, different waveforms are used for each function, and interference between both functions must be mitigated. In the latter, a single waveform is transmitted, and trade-offs are made in the waveform design between both functions. These are also often named Dual Function radar-Communication (DFRC) systems. In order to evaluate the performance of such systems in a given scenario, multiple metrics have been defined for the radar and communication functions. One tool enabling to evaluate these metrics is stochastic geometry.

Stochastic geometry is a branch of mathematics which provides mathematical models and statistical methods to study and analyse random spatial distributions, mainly based on point processes. This tool has been widely used to assess the average performance achieved in wireless networks [4]–[8]. As a non exhaustive list, several performance metrics evaluated with this tool are the coverage probability, spectral efficiency, energy

efficiency and total received power. The joint evaluation of multiple metrics has also been considered, i.e. the achieved rate in uplink and downlink [9], or the simultaneous wireless information and power transfer [10]. For radar applications, it has also been used to evaluate radar metrics (i.e. the false alarm, detection and success probability) and the impact of multiple parameters in different scenarios. For instance, [11] analyses the Cumulative Distribution Function (CDF) of the interference with a population of pulsed-radar devices, [12]–[14] consider the radar performance in a cluttered environment, and [15] evaluates the detection probability when multiple obstacles are distributed around the radar systems. Considering joint radar and communication scenarios, some works have been published regarding either coexisting radar and communication or co-designed systems. In the first case, [16], [17] evaluate the radar range and the communication success probability of a joint radar-communication network with Time Division Multiple Access (TDMA). The interference from a rotating radar sharing the same spectrum as a cellular system is considered in [18], while [19] analyses the interference of a massive Multiple Input Multiple Output (MIMO) cellular network on a radar system. Finally, the development of cooperative multi-point detection is presented in [20], [21]. In the second case with co-designed systems, [22] evaluates the cooperative detection volume of a joint radar and communication system where targets are detected with the main beam and different stations cooperate by communicating through the secondary beams. The increase of the communication throughput with joint radar-communication system is evaluated in [23], and an analytical framework to optimise the system parameters is proposed.

Many automotive scenarios have been studied in a stochastic geometry framework. First, for radar applications only, [24] compares the performance obtained with different random Radar Cross Section (RCS) models. For the position of the vehicles, instead of using Poisson Point Processes (PPP), [25] also proposes to use a one-dimensional lattice, and [26] uses Matérn hard-core processes in two dimensions. In [27], an arbitrary number of lanes in both directions is considered, and the reflected interference from vehicles on neighbour lanes is taken into account. In [28], a multiple lane scenario is also considered, with front- and side-mounted radars with directional antenna patterns. To obtain a fine-grained analysis,

François De Saint Moulin is a Research Fellow of the Fonds de la Recherche Scientifique - FNRS.

[29], [30] evaluate the meta distribution of the Signal to Interference plus Noise Ratio (SINR), which enables to analyse the reliability of the detection at each individual vehicle. Regarding joint radar and communication applications, the cooperative detection range is evaluated in [31] and [32], respectively with spectrum allocation between both functions or with a joint radar-communication system. This range is defined as the total range in which targets are detected by multiple vehicles communicating with each other.

To our best knowledge, the performance of both radar and communication functions in a single DFRC system have not been investigated in a joint manner. This is especially useful when the radar and communication potentially interfere with each other, requiring a joint evaluation of the performance achieved by both functions. In this paper, we consider a two-lane road automotive scenario including crossing vehicles and smart traffic lights, both equipped with DFRC systems. In that scenario, the communication signal from the traffic light and the radar echo interfere with each other. Therefore, we design multiple metrics in order to evaluate separately or simultaneously the performance of both functions, highlight possible trade-offs and optimise multiple parameters as the vehicles and traffic lights powers, or the traffic light density.

Contributions

The contributions of this paper are summarised as follows:

- A new automotive scenario involving smart traffic lights and vehicles equipped with joint radar-communication systems is studied within the stochastic geometry framework. A focus is made on the performance achieved for a typical vehicle receiving a communication signal from the traffic lights while simultaneously detecting the next vehicle in the same lane.
- In that scenario, multiple common metrics are computed, namely
 - the *communication coverage probability*, i.e. the probability for the communication SINR to reach a given requirement;
 - the *radar false alarm probability*, i.e. the probability for the radar receiver to falsely detect a target which doesn't exist;
 - the *radar detection probability*, i.e. the probability for the radar receiver to detect a real target;
 - the *radar success probability*, i.e. the probability for the radar SINR to reach a given requirement.
- Two new joint metrics are designed to evaluate the performance for both radar and communication functions, namely
 - the *Joint Radar Detection and Communication Coverage Probability* (JRDCCP), i.e. the probability to detect a target with a given false alarm probability at the radar function, while achieving a sufficient SINR at the communication function;
 - the *Joint Radar Success and Communication Coverage Probability* (JRSCCP), i.e. the probability to

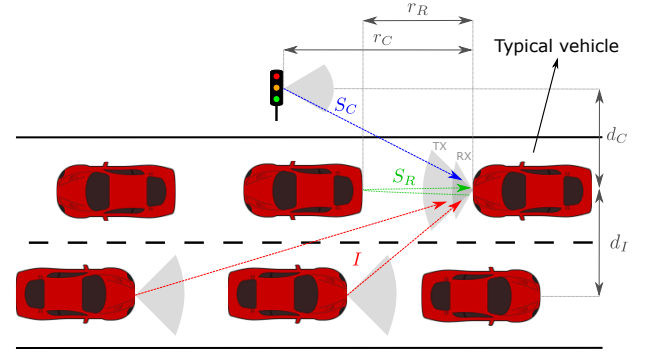


Fig. 1. Considered two-lane road scenario.

achieve simultaneously a sufficient SINR at both radar and communication functions.

Additionally, power optimisation for both vehicles and traffic lights is performed.

- Upper and lower bounds are proposed for the joint metrics, and conditional metrics are also defined, namely
 - the coverage probability for vehicles already achieving a given detection or success probability;
 - the detection or success probability for vehicles already achieving a given coverage probability.
- A new tractable model is proposed to integrate perfect or partial interference cancellation at the radar and communication functions when they cooperate with each other. All proposed metrics are extended to include the latter.

II. SYSTEM MODEL

A. Considered scenario

We consider a two-lane road scenario, as illustrated in Figure 1. The typical vehicle is equipped at the front side with a DFRC system. Their transmit power, transmit antenna beamwidth and receive antenna beamwidth are respectively denoted as P_V , ψ_{VT} and ψ_{VR} . The typical vehicle receives a radar echo coming from the first vehicle driving in the same lane, and a communication signal from the nearest traffic light ahead. The transmit power and transmit antenna beamwidth of this light are respectively denoted as P_L and ψ_{LT} . The vehicles driving in the opposite direction are interfering with the radar echo and communication signal. The distance perpendicular to the road direction between the typical vehicle and the smart traffic light (resp. the center of the opposite lane) is denoted d_C (resp. d_I).

Vehicles driving in the same way, interfering vehicles on the opposite way, and traffic lights are distributed on three parallel lines following three independent PPPs Φ_R , Φ_I and Φ_L of intensities respectively given by

$$\begin{aligned}\lambda_R(r) &= \lambda_V \mathbb{1}(r_{Rmin} \leq r \leq r_{Rmax}), \\ \lambda_I(r) &= \lambda_I \mathbb{1}(r_{Imin} \leq r), \\ \lambda_L(r) &= \lambda_L \mathbb{1}(r_{Cmin} \leq r),\end{aligned}\tag{1}$$

where λ_V , λ_I and λ_L are respectively the densities of vehicles driving on the same lane as the typical vehicle, interfering

vehicles and traffic lights. The minimum and maximum detectable range of the radar function, the minimum distance (parallel to the road) of the communication signal and the minimum distance (parallel to the road) of the interfering signals are respectively denoted by $r_{R\min}$, $r_{R\max}$, $r_{C\min}$ and $r_{I\min}$. Note that $\lambda_I \neq \lambda_V$ since we assume that the vehicles in the opposite lane are not always interfering; either the different vehicles transmit asynchronously, or they are not all equipped with DFRC systems. Additionally, $r_{C\min}$ and $r_{I\min}$ are directly related to the antenna beamwidths of the different systems: $r_{C\min} = d_C / \tan(\min(\psi_{LT}, \psi_{VR})/2)$ and $r_{I\min} = d_I / \tan(\min(\psi_{VT}, \psi_{VR})/2)$.

B. Propagation models

Let us consider a linear path-loss model $[L_k]_{\text{dB}} = [\beta_k]_{\text{dB}} + 10\alpha_k \log_{10}(r)$, where $k = \{R, C, I\}$ designates the considered link, α_k is the path-loss exponent and β_k is the intercept. The received power for the communication link is given by the Friis equation [33] as

$$S_C(r) = P_L G_C \frac{c^2}{4\pi f_c^2} L_C^{-1} \left(\sqrt{r^2 + d_C^2} \right) = \rho_C (r^2 + d_C^2)^{-\frac{\alpha_C}{2}} \quad (2)$$

at a distance r (parallel to the road), with $\rho_C = \frac{P_L G_C c^2}{4\pi f_c^2 \beta_C}$. The speed of light is denoted by c , and the carrier frequency by f_c , and G_C is the beamforming gain of the communication link. The interfering power is obtained in the same manner:

$$\begin{aligned} I &= \sum_{i | \phi_i \in \Phi_I} P_V G_I \frac{c^2}{4\pi f_c^2} L_I^{-1} \left(\sqrt{\|\phi_i\|^2 + d_I^2} \right) |h_i|^2 \\ &= \sum_{i | \phi_i \in \Phi_I} \rho_I (\|\phi_i\|^2 + d_I^2)^{-\frac{\alpha_I}{2}} |h_i|^2, \end{aligned} \quad (3)$$

where $\rho_I = \frac{P_V G_I c^2}{4\pi f_c^2 \beta_I}$. The beamforming gain of the interfering links is denoted by G_I , and $|h_i|^2$ are i.i.d. Rician distributed small-scale fading random variables. Note that the small-scale fading has been neglected for the communication link for tractability. However, it is supposed to be highly rician since the traffic light is located at the same side of the road (and not in the traffic as the interfering links), and high frequencies (24/77GHz) are considered for this application.

In the literature, the received power for the radar link is usually given by the radar equation [34]:

$$S_{R,\text{RCS}}(r) = P_V G_R \frac{c^2}{4\pi f_c^2} L_R^{-2}(r) \sigma \quad (4)$$

with a distance r between the radar and the target, where σ is the RCS of the target, and G_R is the beamforming gain of the radar link. However, the RCS varies with the distance to the target, its geometry and the considered frequencies. The issue is often tackled by modelling the RCS as an exponentially distributed random variable, following the Swerling I model. Additionally, this model is only valid in far field, i.e. when $r \geq \frac{2D^2 f_c}{c}$ with D the largest dimension of the reflector. For instance, at a distance of 5m, it requires reflectors with largest

dimensions $D \leq \sqrt{\frac{rc}{2f_c}} \approx 18\text{cm}$ or 10cm respectively at carrier frequencies of 24 and 77GHz. To alleviate the issues inherent to the RCS-based model, we instead modelled the received power for the radar link as

$$S_R(r) = P_V G_R \frac{c^2}{4\pi f_c^2} L_R^{-1}(2r) = \rho_R r^{-\alpha_R} \quad (5)$$

with a distance r between the radar and the target. This model is only valid for reflector dimensions larger than the first Fresnel zones diameter, namely $D \geq \sqrt{\frac{rc}{f_c}} \approx 25$ or 14cm at a distance of 5m, and carrier frequencies of 24 and 77GHz. Therefore, it is suited for the considered automotive scenario. Again, the small-scale fading is neglected for tractability, but it is also supposed to be highly rician considering the scenario and the high frequencies used in automotive radar applications.

To simplify the notations, we define $S_R \equiv S_R(r_R)$ where r_R is the distance between the vehicle of interest and the vehicle driving ahead, and $S_C \equiv S_C(r_C)$, where r_C is the distance (parallel to the road) between the vehicle of interest and the nearest traffic light ahead. We also define $S_{R\min} = S_R(r_{R\max})$, $S_{R\max} = S_R(r_{R\min})$ and $S_{C\max} = S_C(r_{C\min})$ as the minimum and maximum possible power levels for the radar and communication links. Let us also define the following operator:

$$\mathcal{E}^A [g(S_R, S_C)] = \mathbb{E}_{S_R, S_C} [g(S_R, S_C) \cdot \mathbb{1}((S_R, S_C) \in A)]$$

which computes the expectation over S_R and S_C of a function g in a given domain $A \in \mathbb{R}^2$.

III. DEVELOPMENT OF THE METRICS

In this section, multiple metrics are presented and developed, following the different steps of Figure 2.

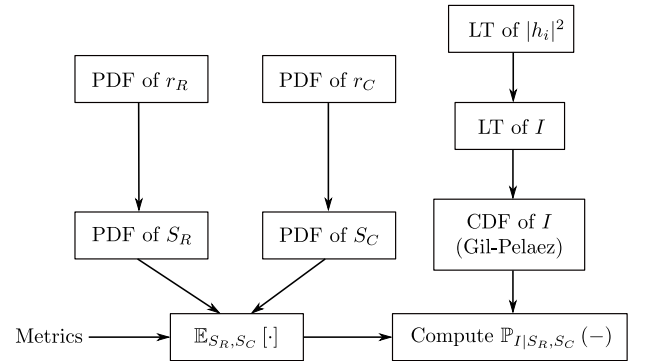


Fig. 2. Metrics development steps.

First, the Probability Density Functions (PDF) of r_R and r_C are computed. Then, the PDFs of S_R and S_C are derived from the PDFs of their associated distances. This enables to condition the metrics over the powers of the useful signals, and develop their expressions to obtain a function of the CDF of I . Finally, this CDF is computed based on the Laplace Transform (LT) of I — itself function of the LT of the small-scale fading of the interfering links $|h_i|^2$ — thanks to the Gil-Pelaez theorem [35].

In Sections III-A to III-D, all preliminary results needed in order to develop the metrics are computed. Next, usual radar and communication metrics, namely

- 1) the communication coverage probability;
- 2) the radar detection and false alarm probabilities;
- 3) the radar success probability,

are presented and derived in Sections III-E to III-G. Then, based on these different metrics, the two joint metrics, namely

- 1) the JRDCCP metric;
- 2) the JRSCCP metric,

are designed in Sections III-H and III-I. Upper and lower bounds are also proposed. Finally, conditional metrics are defined in Section III-J based on the given radar, communication and joint metrics.

A. Probability density functions of r_R and r_C

Based on the densities given in (1), the PDFs of r_R and r_C are presented in Lemma 1.

Lemma 1: Assuming that there is at least one vehicle in the radar detectable range, the PDFs of r_R and r_C are respectively given by

$$f_{r_R}(r) = \frac{\lambda_V \exp(-\lambda_V(r - r_{Rmin}))}{1 - \exp(-\lambda_V(r_{Rmax} - r_{Rmin}))} \cdot \mathbb{1}(r_{Rmin} \leq r \leq r_{Rmax}) \quad (6)$$

and

$$f_{r_C}(r) = \lambda_L \exp(-\lambda_L(r - r_{Cmin})) \cdot \mathbb{1}(r_{Cmin} \leq r). \quad (7)$$

Proof: The proof is detailed in Appendix A. ■

B. Probability density functions of S_R and S_C

Based on the expressions of Lemma 1, the expressions of the PDFs of S_R and S_C are developed in Lemma 2.

Lemma 2: Assuming that there is at least one vehicle in the radar detectable range, the PDFs of S_R and S_C are respectively given by

$$f_{S_R}(s) = \frac{r_R(s)}{\alpha_R s} \frac{\lambda_V \exp(-\lambda_V(r_R(s) - r_{Rmin}))}{1 - \exp(-\lambda_V(r_{Rmax} - r_{Rmin}))} \cdot \mathbb{1}(S_{Rmin} \leq s \leq S_{Rmax}) \quad (8)$$

with $r_R(s) = \rho_R^{\frac{1}{\alpha_R}} s^{-\frac{1}{\alpha_R}}$, and

$$f_{S_C}(s) = \frac{r_C^2(s) + d_C^2}{\alpha_C s r_C(s)} \lambda_L \exp(-\lambda_L(r_C(s) - r_{Cmin})) \cdot \mathbb{1}(0 \leq s \leq S_{Cmax}) \quad (9)$$

with $r_C(s) = \sqrt{\rho_C^{\frac{2}{\alpha_C}} s^{-\frac{2}{\alpha_C}} - d_C^2}$.

Proof: The proof is detailed in Appendix B. ■

C. Laplace transform of the small-scale fading for the interfering links

Under Rician fading, the Laplace transform of the small-scale fading random variables is given by Lemma 3.

Lemma 3: The Laplace transform of the small-scale fading for the interfering links is given by

$$\mathcal{L}_{|h_i|^2}(s) = \frac{K+1}{K+1+s} \exp\left(-\frac{Ks}{K+1+s}\right), \quad (10)$$

where K is the Rician K -factor of the interfering links.

Proof: The proof is detailed in Appendix C. ■

D. Laplace transform of the interfering power I

Based on Lemma 3, the expression of the Laplace transform of the interfering power I is obtained in Lemma 4.

Lemma 4: The Laplace transform of the interfering power I is given by

$$\mathcal{L}_I(s) = \exp\left(-\lambda_I \int_{r_{Imin}}^{\infty} \left(1 - \mathcal{L}_{|h_i|^2}\left(s\rho_I(r^2 + d_I^2)^{-\frac{\alpha_I}{2}}\right)\right) dr\right), \quad (11)$$

where $\mathcal{L}_{|h_i|^2}$ denotes the Laplace transform of the small-scale fading for the interfering links.

Proof: The proof is detailed in Appendix D. ■

E. Coverage probability

The coverage probability is defined as the probability to achieve a sufficient SINR for the communication function. Additionally, ensuring that the SINR is higher than θ also ensures that the achievable communication rate is higher than $\frac{1}{T_c} \log_2(1 + \theta)$ where $1/T_c$ is the symbol rate of the transmission.

In the considered scenario, the radar echo from the next vehicle ahead and the vehicles on the opposite lane are interfering with the communication function. Assuming that the scenario is interference-limited, this metric is written as

$$\mathcal{P}_C(\theta) = \mathbb{P}\left(\frac{S_C}{S_R + I} \geq \theta\right). \quad (12)$$

Proposition 1 gives the expression of the coverage probability depending on the required communication Signal to Interference Ratio (SIR) threshold.

Proposition 1: For a given communication SIR threshold θ , the coverage probability is obtained as

$$\mathcal{P}_C(\theta) = \mathcal{E}^{\Xi_C} \left[\frac{1}{2} - \frac{1}{\pi} \int_0^{\infty} \frac{1}{\tau} \text{Im} \{ \mathcal{L}_I(-j\tau) \xi_C(\tau) \} d\tau \right] \quad (13)$$

where

$$\xi_C(\tau) = \exp\left(-j\tau \left(\frac{S_C}{\theta} - S_R\right)\right) \quad (14)$$

and the area Ξ_C is defined as

$$\Xi_C \triangleq \left\{ \begin{array}{l} S_{Rmin} \leq S_R \leq S_{Rmax} \\ \theta S_R \leq S_C \leq S_{Cmax} \end{array} \right\}. \quad (15)$$

Proof: The proof is detailed in Appendix F-B. ■

Note that the CDF of the *spectral efficiency* can be computed based on the coverage probability:

$$\mathcal{R}(\eta) = \mathbb{P} \left(\log_2 \left(1 + \frac{S_C}{S_R + I} \right) \geq \eta \right) = \mathcal{P}_C(2^\eta - 1). \quad (16)$$

Similarly, the average spectral efficiency is computed as

$$\bar{\mathcal{R}} = \int_0^\infty \mathcal{R}(\eta) d\eta = \frac{1}{\ln 2} \int_0^\infty \frac{\mathcal{P}_C(\theta)}{1 + \theta} d\theta, \quad (17)$$

applying the change of variable $\theta = 2^\eta - 1$.

F. Detection and false alarm probabilities

Let us consider the output of the radar receiver before the detector. As done in [34], two hypotheses are defined for each cell, i.e. each element of the delay-Doppler-angle map produced at its output:

- H_0 : there is no target within the cell;
- H_1 : there is a target within the cell.

The amplitude of the cell under test is described as

$$x = \begin{cases} A + w & \text{under } H_1, \\ w & \text{under } H_0, \end{cases} \quad (18)$$

where $|A|^2 = S_R \kappa$ with a radar processing gain κ , w is an Additive White Gaussian Noise (AWGN) of variance σ_w^2 modelling the noise and the interference. For a given threshold γ , the *false alarm probability* \mathcal{P}_{FA} and *detection probability* \mathcal{P}_D are respectively defined as

$$\mathcal{P}_{FA}(\gamma) = \mathbb{P}_x(|x|^2 \geq \gamma | H_0), \quad (19)$$

$$\mathcal{P}_D(\gamma) = \mathbb{P}_x(|x|^2 \geq \gamma | H_1). \quad (20)$$

In practice, a given false alarm probability is required, and the threshold is defined to meet this requirement.

In the considered automotive scenario, the nearest traffic light ahead and the vehicles on the opposite lane are interfering with the radar function. Assuming that the scenario is interference-limited, these metrics are respectively rewritten as follows:

$$\mathcal{P}_{FA}(\gamma) = \mathbb{P}_{S_C, I}(S_C + I \geq \gamma), \quad (21)$$

$$\mathcal{P}_D(\gamma) = \mathbb{P}(S_R \kappa + S_C + I \geq \gamma). \quad (22)$$

Propositions 2 and 3 provide expressions of the false alarm and detection probabilities depending on the threshold of the radar detector.

Proposition 2: For a given threshold γ , the false alarm probability is given by

$$\mathcal{P}_{FA}(\gamma) = 1 - \mathcal{E}^{\Xi_F} \left[\frac{1}{2} - \frac{1}{\pi} \int_0^\infty \frac{1}{\tau} \text{Im} \{ \mathcal{L}_I(-j\tau) \xi_F(\tau, s) \} d\tau \right] \quad (23)$$

where

$$\xi_F(\tau) = \exp(-j\tau(\gamma - S_C)), \quad (24)$$

and the area Ξ_F is defined as

$$\Xi_F \triangleq \left\{ \begin{array}{l} S_C \leq \gamma \\ 0 \leq S_C \leq S_{Cmax} \end{array} \right\}. \quad (25)$$

Proof: The proof is detailed in Appendix E-C. ■

Proposition 3: For a given threshold γ , the detection probability is given by

$$\mathcal{P}_D(\gamma) = 1 - \mathcal{E}^{\Xi_D} \left[\frac{1}{2} - \frac{1}{\pi} \int_0^\infty \frac{1}{\tau} \text{Im} \{ \mathcal{L}_I(-j\tau) \xi_D(\tau) \} d\tau \right] \quad (26)$$

where

$$\xi_D(\tau) = \exp(-j\tau(\gamma - S_R \kappa - S_C)), \quad (27)$$

and the area Ξ_D is defined as

$$\Xi_D \triangleq \left\{ \begin{array}{l} S_C \leq \gamma - S_R \kappa \\ S_{Rmin} \leq S_R \leq S_{Rmax} \\ 0 \leq S_C \leq S_{Cmax} \end{array} \right\}. \quad (28)$$

Proof: The proof is detailed in Appendix E-B. ■

G. Success probability

Following the hypothesis testing problem presented in Section III-F, for a given false alarm probability \mathcal{P}_{FA} , the detection probability is given by [34]

$$\mathcal{P}_D = Q_1 \left(\sqrt{2|A|^2/\sigma_w^2}, \sqrt{-2 \ln \mathcal{P}_{FA}} \right), \quad (29)$$

where Q_1 is the first order Marcum Q-function. Therefore, since an increase of the radar SINR leads to a higher detection probability, the *success probability* has been defined as

$$\mathcal{P}_S(\theta') = \mathbb{P}(|A|^2/\sigma_w^2 \geq \theta') \quad (30)$$

where θ' is a given radar SINR threshold.

In the considered automotive scenario, the nearest traffic light ahead and the vehicles on the opposite lane interfere with the radar function. Assuming that the scenario is interference-limited, this metric is rewritten as follows:

$$\mathcal{P}_S(\theta') = \mathbb{P} \left(\frac{S_R \kappa}{S_C + I} \geq \theta' \right). \quad (31)$$

Proposition 4 gives the expression of the success probability depending on the required radar SIR threshold.

Proposition 4: For a given radar SIR threshold θ' , the success probability is obtained as

$$\mathcal{P}_S(\theta') = \mathcal{E}^{\Xi_S} \left[\frac{1}{2} - \frac{1}{\pi} \int_0^\infty \frac{1}{\tau} \text{Im} \{ \mathcal{L}_I(-j\tau) \xi_S(\tau) \} d\tau \right] \quad (32)$$

where

$$\xi_S(\tau) = \exp\left(-j\tau\left(\frac{S_R\kappa}{\theta'} - S_C\right)\right), \quad (33)$$

and the area Ξ_S is defined as

$$\Xi_S \triangleq \left\{ \begin{array}{l} S_C \leq S_R\kappa/\theta' \\ S_{Rmin} \leq S_R \leq S_{Rmax} \\ 0 \leq S_C \leq S_{Cmax} \end{array} \right\}. \quad (34)$$

Proof: The proof is detailed in Appendix F-C. ■

H. JRDCCP metric

We define the JRDCCP metric as an extension of the communication coverage and the radar detection probabilities for radar-communication scenarios:

$$\mathcal{D}(\theta; \gamma) = \mathbb{P}\left(S_R\kappa + S_C + I \geq \gamma, \frac{S_C}{S_R + I} \geq \theta\right) \quad (35)$$

for a given $\mathcal{P}_{FA}(\gamma)$.

This gives the probability that a radar detection occurs for a given false alarm probability, while ensuring a sufficient SIR for the communication function. The threshold γ is selected in order to fulfill the false alarm probability requirement, and the JRDCCP metric is then obtained for a given communication SIR threshold θ . The metric is developed in Proposition 5.

Proposition 5: For a given false alarm probability \mathcal{P}_{FA} (and therefore for a given threshold γ) and a given communication SIR threshold θ , the JRDCCP metric is obtained as

$$\begin{aligned} \mathcal{D}(\theta; \gamma) = & -\mathcal{E}^{\Omega_{D2}} \left[\frac{1}{\pi} \int_0^\infty \frac{1}{\tau} \text{Im} \{ \mathcal{L}_I(-j\tau) \psi_{D2}(\tau) \} d\tau \right] \\ & + \mathcal{E}^{\Omega_{D1}} \left[\frac{1}{2} - \frac{1}{\pi} \int_0^\infty \frac{1}{\tau} \text{Im} \{ \mathcal{L}_I(-j\tau) \psi_{D1}(\tau) \} d\tau \right] \end{aligned} \quad (36)$$

where

$$\psi_{D1}(\tau) = \xi_C(\tau), \quad \psi_{D2}(\tau) = \xi_C(\tau) - \xi_D(\tau), \quad (37)$$

and the areas Ω_{D1} and Ω_{D2} are defined as

$$\Omega_{D1} \triangleq \left\{ \begin{array}{l} S_C \leq \max(\theta S_R, \gamma - S_R\kappa) \\ S_{Rmin} \leq S_R \leq S_{Rmax} \\ 0 \leq S_C \leq S_{Cmax} \end{array} \right\}, \quad (38)$$

$$\Omega_{D2} \triangleq \left\{ \begin{array}{l} \frac{\theta\gamma}{\theta+1} - S_R \frac{\theta(\kappa-1)}{\theta+1} \leq S_C \leq \gamma - \kappa S_R \\ S_{Rmin} \leq S_R \leq S_{Rmax} \\ 0 \leq S_C \leq S_{Cmax} \end{array} \right\}. \quad (39)$$

Proof: The proof is detailed in Appendix E-A. ■

I. JRSCCP metric

We define the JRSCCP metric as an extension of the success probability for radar-communication scenarios:

$$\mathcal{S}(\theta', \theta) = \mathbb{P}\left(\frac{S_R\kappa}{S_C + I} \geq \theta', \frac{S_C}{S_R + I} \geq \theta\right). \quad (40)$$

It gives the probability that both the radar and communication SIRs are sufficient compared to the threshold requirements. This metric is developed in Proposition 6.

Proposition 6: For a given radar SIR threshold θ' and communication SIR threshold θ , if the following condition is fulfilled:

$$[\theta']_{dB} + [\theta]_{dB} \leq [\kappa]_{dB}, \quad (41)$$

the JRSCCP metric is obtained as

$$\begin{aligned} \mathcal{S}(\theta', \theta) = & \mathcal{E}^{\Omega_{S1}} \left[\frac{1}{2} - \frac{1}{\pi} \int_0^\infty \frac{1}{\tau} \text{Im} \{ \mathcal{L}_I(-j\tau) \psi_{S1}(\tau) \} d\tau \right] \\ & + \mathcal{E}^{\Omega_{S2}} \left[\frac{1}{2} - \frac{1}{\pi} \int_0^\infty \frac{1}{\tau} \text{Im} \{ \mathcal{L}_I(-j\tau) \psi_{S2}(\tau) \} d\tau \right] \end{aligned} \quad (42)$$

where

$$\psi_{S1}(\tau) = \xi_S(\tau), \quad \psi_{S2}(\tau) = \xi_C(\tau), \quad (43)$$

and the areas Ω_{S1} and Ω_{S2} are defined as

$$\Omega_{S1} \triangleq \left\{ \begin{array}{l} S_R \frac{\theta(\theta' + \kappa)}{\theta'(\theta + 1)} \leq S_C \leq \frac{S_R\kappa}{\theta'} \\ S_{Rmin} \leq S_R \leq S_{Rmax} \\ 0 \leq S_C \leq S_{Cmax} \end{array} \right\}, \quad (44)$$

$$\Omega_{S2} \triangleq \left\{ \begin{array}{l} \theta S_R \leq S_C \leq S_R \frac{\theta(\theta' + \kappa)}{\theta'(\theta + 1)} \\ S_{Rmin} \leq S_R \leq S_{Rmax} \\ 0 \leq S_C \leq S_{Cmax} \end{array} \right\}. \quad (45)$$

Otherwise, the metric is equal to zero.

Proof: The proof is detailed in Appendix F-A. ■

Using Fréchet inequalities [36], upper and lower bounds are proposed for the JRDCCP and JRSCCP metrics in Corollary 1.

Corollary 1: For a given false alarm probability \mathcal{P}_{FA} (and therefore for a given threshold γ) and a given communication SIR threshold θ , the JRDCCP metric is bounded by

$$\mathcal{D}_m(\theta; \gamma) \leq \mathcal{D}(\theta; \gamma) \leq \mathcal{D}_M(\theta; \gamma), \quad (46)$$

with

$$\mathcal{D}_m(\theta; \gamma) = \max(0, \mathcal{P}_D(\gamma) + \mathcal{P}_C(\theta) - 1), \quad (47)$$

$$\mathcal{D}_M(\theta; \gamma) = \min(\mathcal{P}_D(\gamma), \mathcal{P}_C(\theta)). \quad (48)$$

Similarly, for a given radar SIR threshold θ' and communication SIR threshold θ , the JRSCCP metric is bounded by

$$\mathcal{S}_m(\theta', \theta) \leq \mathcal{S}(\theta', \theta) \leq \mathcal{S}_M(\theta', \theta), \quad (49)$$

with

$$S_m(\theta', \theta) = \max(0, \mathcal{P}_S(\theta') + \mathcal{P}_C(\theta) - 1), \quad (50)$$

$$S_M(\theta', \theta) = \min(\mathcal{P}_S(\theta'), \mathcal{P}_C(\theta)). \quad (51)$$

Proof: The proposed bounds are given by Fréchet inequalities. ■

J. Conditional metrics

One can be interested in the performance achieved by vehicles already fulfilling successfully one of the two functions. On the one hand, for the radar function, it is supposed that either a radar detection has occurred, or that the radar SIR fulfills a given threshold requirement. Conditional metrics are then respectively expressed as follows:

$$\mathcal{P}_{C|D}(\theta; \gamma) = \mathbb{P} \left(\frac{S_C}{S_R + I} \geq \theta \mid S_R \kappa + S_C + I \geq \gamma \right) \quad (52)$$

for a given $\mathcal{P}_{FA}(\gamma)$,

$$\mathcal{P}_{C|S}(\theta'; \theta) = \mathbb{P} \left(\frac{S_C}{S_R + I} \geq \theta \mid \frac{S_R \kappa}{S_C + I} \geq \theta' \right). \quad (53)$$

On the other hand, for the communication function, it is supposed that the communication SIR fulfills a given threshold requirement. Conditional metrics are then expressed as follows:

$$\mathcal{P}_{D|C}(\gamma; \theta) = \mathbb{P} \left(S_R \kappa + S_C + I \geq \gamma \mid \frac{S_C}{S_R + I} \geq \theta \right) \quad (54)$$

for a given $\mathcal{P}_{FA}(\gamma)$,

$$\mathcal{P}_{S|C}(\theta'; \theta) = \mathbb{P} \left(\frac{S_R \kappa}{S_C + I} \geq \theta' \mid \frac{S_C}{S_R + I} \geq \theta \right). \quad (55)$$

The different conditional metrics are detailed in Corollary 2.

Corollary 2: For a given false alarm probability \mathcal{P}_{FA} (and therefore for a given threshold γ) or a given radar SIR threshold θ' , the coverage probabilities achieved by vehicles performing successfully the radar function for a given communication SIR threshold θ are given by

$$\mathcal{P}_{C|D}(\theta; \gamma) = \mathcal{D}(\theta; \gamma) / \mathcal{P}_D(\gamma) \quad (56)$$

and

$$\mathcal{P}_{C|S}(\theta; \theta') = \mathcal{S}(\theta', \theta) / \mathcal{P}_S(\theta'). \quad (57)$$

Similarly, the detection and success probabilities achieved by vehicles performing successfully the communication function are given by

$$\mathcal{P}_{D|C}(\gamma; \theta) = \mathcal{D}(\theta; \gamma) / \mathcal{P}_C(\theta) \quad (58)$$

and

$$\mathcal{P}_{S|C}(\theta'; \theta) = \mathcal{S}(\theta', \theta) / \mathcal{P}_C(\theta). \quad (59)$$

Proof: These results are obtained using Bayes law. ■

Note that the average spectral efficiency can also be evaluated for these users following (17):

$$\bar{\mathcal{R}}_{|D} = \frac{1}{\ln 2} \int_0^\infty \frac{\mathcal{P}_{C|D}(x)}{1+x} dx,$$

$$\bar{\mathcal{R}}_{|S} = \frac{1}{\ln 2} \int_0^\infty \frac{\mathcal{P}_{C|S}(x)}{1+x} dx.$$

IV. NUMERICAL ANALYSIS

Table I summarises the parameters used in the simulated scenarios.

TABLE I
SCENARIO PARAMETERS.

| | |
|--|---|
| $P_V = P_L = 1\text{W}$ | $G_R = G_C = G_I = 1$ |
| $\kappa = 1$ | $d_C = 2.5\text{m}, d_I = 3\text{m}$ |
| $r_{R\min} = 5\text{m}, \psi_{VT} = 22.5^\circ, \psi_{VR} = \psi_{LT} = 45^\circ$ | |
| $\lambda_V = 0.02\text{m}^{-1}, \lambda_L = 0.01\text{m}^{-1}, \lambda_I = 0.002\text{m}^{-1}$ | |
| $\beta_R = \beta_C = \beta_I = 4\pi$ | $\alpha_R = 2, \alpha_C = \alpha_I = 3$ |

A. Metrics analysis

Figure 3 illustrates the false alarm probability, the detection probability and the JRDCCP metric, obtained with stochastic geometry and Monte-Carlo simulations, which are superimposed with each other. Following expressions in (22), the false alarm probability is always lower than the detection probability at any threshold. The false alarm and detection probability decrease to zero when the radar threshold increases. Therefore, the number of false alarms is lowered at the price of less detections.

For low values of γ (corresponding to high false alarm probabilities), the detection probability is close to one, and the JRDCCP metric tends to be equal to the communication coverage probability. Contrariwise, for low values of the communication SIR threshold θ , the communication coverage probability is close to one and the JRDCCP metric tends to be equal to the detection probability. The same behaviour is obtained with the JRSCCP metric, shown in Figure 4. Again, results obtained with stochastic geometry and Monte-Carlo simulations are superimposed. For low values of the radar SIR threshold θ' , the radar success probability is close to one and the JRSCCP tends to be equal to the coverage probability. By contrast, for low values of θ , the coverage probability is close to one, and the JRSCCP tends to be equal to the radar success probability. Additionally, the condition given in (41) is verified: with a radar processing gain set to one, whatever the values of θ' and θ , the metric decreases to zero when the sum (in dB) exceeds 0dB. Owing to the negative impact of the communication signal on the radar function and vice-versa, this directly expresses that a trade-off should be achieved.

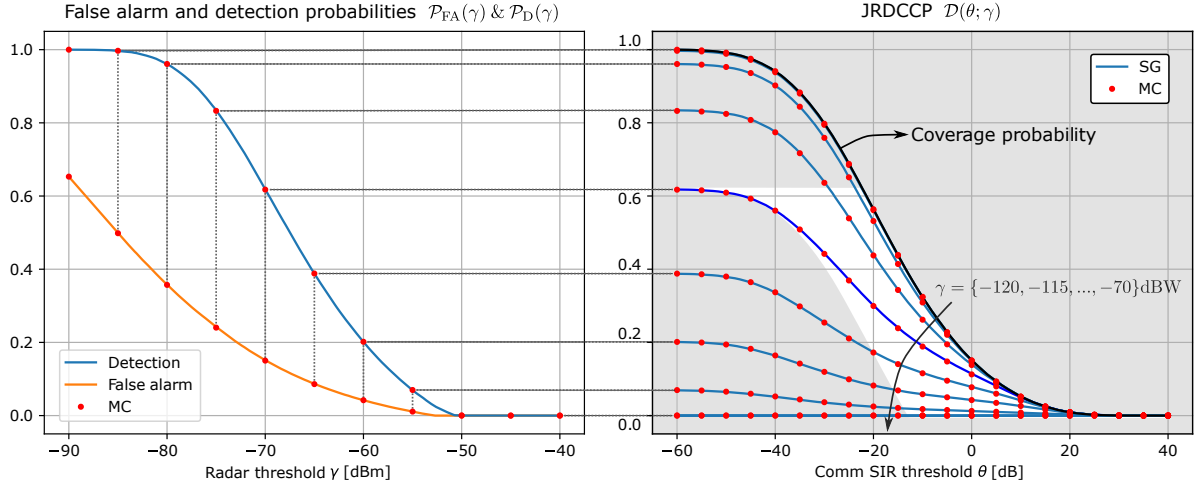


Fig. 3. False alarm probability, detection probability (left) and JRDCCP metric (right). The white area corresponds to the region delimited by the upper and lower bounds of the magenta curve.

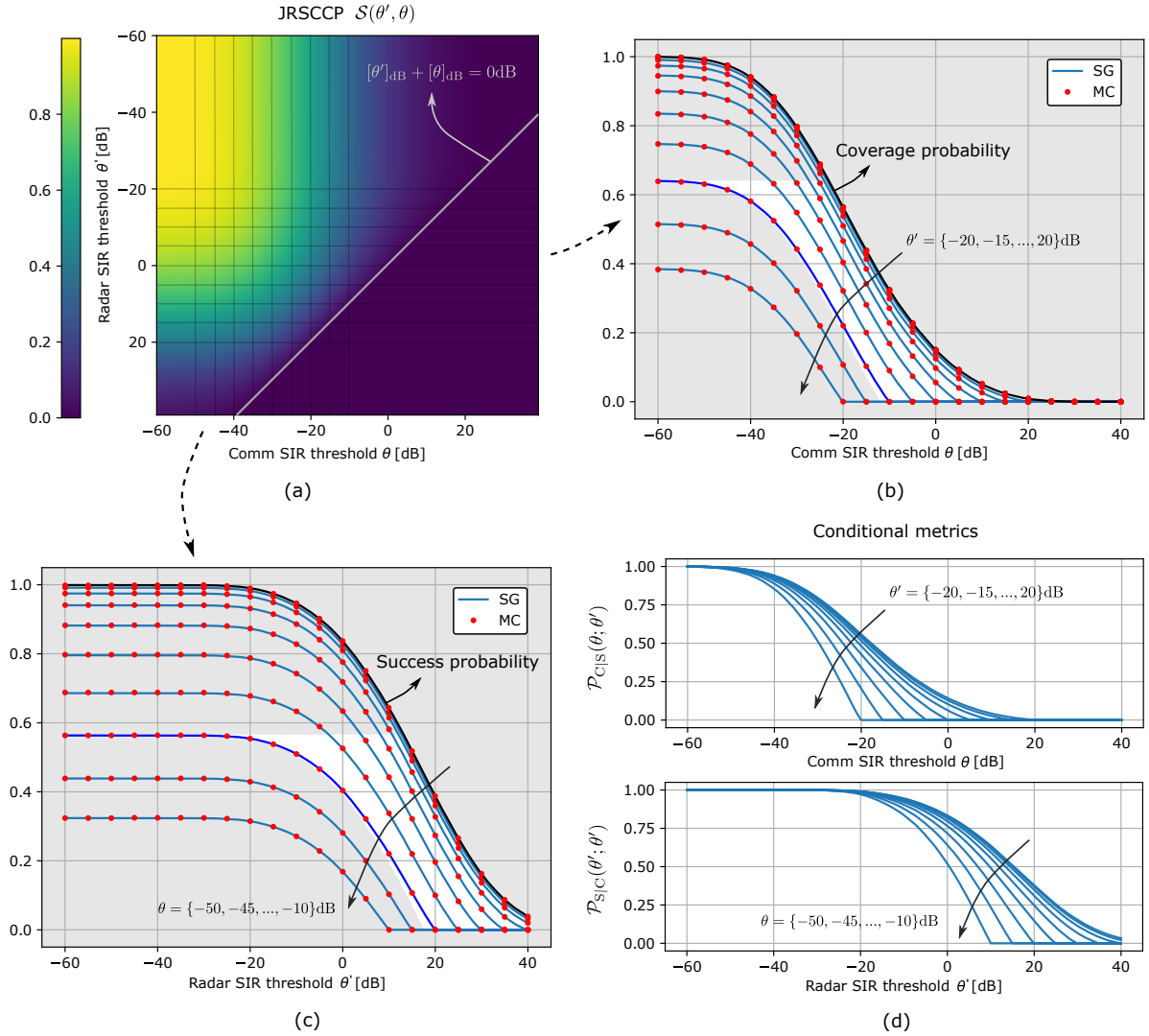


Fig. 4. JRSCCP metric (a), cut along the θ -axis (b), cut along the θ' -axis (c) and conditional metrics (d). The white areas in (b) and (c) correspond to the regions delimited by the upper and lower bounds of the magenta curves.

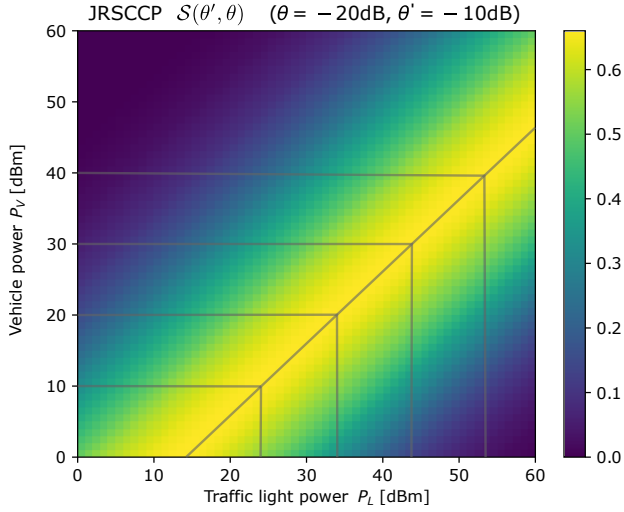


Fig. 5. JRSCCP vs transmitted powers, with $\theta' = -10\text{dB}$ and $\theta = -20\text{dB}$.

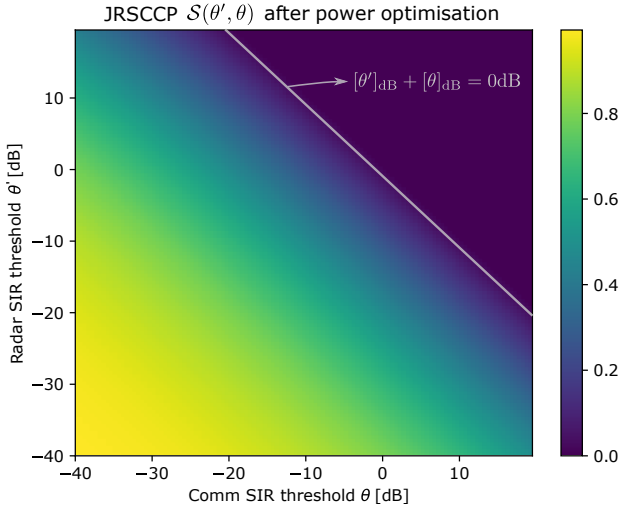


Fig. 6. JRSCCP for different radar and communication SIR thresholds θ' and θ , with traffic light and vehicle powers optimised for each pair of thresholds. The minimum and maximum powers are $P_{Lm} = P_{Vm} = 0\text{dBm}$ and $P_{LM} = P_{VM} = 60\text{dBm}$.

Two conditional metrics are also illustrated in Figure 4d, in which the same condition applies: among the vehicle achieving at least a communication (resp. radar) SIR θ (resp. θ') in dB, there is a zero probability of achieving a radar (resp. communication) SIR higher than $-\theta$ (resp. $-\theta'$) in dB.

Upper and lower bounds are illustrated in both graphs for one curve (dark blue). In both cases, the bounds become tighter as the joint metrics are evaluated for lower thresholds. In these cases, the joint metrics tend to be equal to radar or communication metrics (detection, success and coverage probabilities) and the bounds merge on the metrics.

B. Optimisation of the power levels

Using the joint metrics, optimisation w.r.t. the traffic light and vehicle powers can be performed. For instance, with the

JRSCCP metric, the optimisation problem is formulated for given radar and communication SIR thresholds θ' and θ as

$$\begin{aligned} P_L^*, P_V^* &= \arg \max_{P_L, P_V} \mathcal{S}(\theta', \theta; P_L, P_V) \\ \text{s.t.} \quad &P_{Lm} \leq P_L \leq P_{LM}, \\ &P_{Vm} \leq P_V \leq P_{VM}. \end{aligned} \quad (60)$$

Minimum and maximum values for both traffic light and vehicle powers are respectively denoted by P_{Lm} , P_{LM} , P_{Vm} and P_{VM} .

Figure 5 illustrates how the JRSCCP metric evolves for different transmitted powers P_V and P_L at given SIR thresholds θ and θ' . The power of the smart traffic lights should increase linearly in dB scale with the vehicle power to optimise the joint metric. Indeed, under the interference-limited scenario assumption, the JRSCCP metric can be expressed as a function of the ratio between the traffic light and vehicle powers.

For a given vehicle power, if the communication power is too low, the communication function does not perform well and the joint metric decreases. However, if the communication power is too high, the communication function performs well, but the radar function is impacted and the metric also decreases. Note that an increase of the vehicle power also leads to an increased interference for the radar function, while an increase of the traffic light power only improves the communication SIR in the considered scenario. Note that similar observations can be performed with the traffic light density: an increased density leads to a higher probability for the nearest traffic light to be close. Therefore, the communication power is higher, increasing the communication SIR, but also the interference at the radar function.

The achieved JRSCCP metric after power optimisation is illustrated in Figure 6, for power levels comprised between 0 and 60dBm. Indeed, the achieved performance is higher when low SIR thresholds are required. The condition of (41) is also visible: the JRSCCP metric cannot exceed zero if the SIR threshold requirements are too high. Surprisingly, the metric is symmetric w.r.t. each threshold. It is observed when the interference is low compared to the radar and communication signals. This is happening in most cases with parameters of Table I.

V. EXTENSION WITH INTERFERENCE CANCELLATION

From the radar point of view, any communication signal arriving at the receiver is an interfering signal. From the communication point of view, any unwanted communication signal reaching the receiver is interfering, but the radar echoes coming back to the DFRC transmitter are also considered as interference. Enabling some cooperation between both functions, communication signals which are decoded at the communication receiver could be (partially) suppressed at the radar receiver, and radar echoes which are processed at the radar receiver could be (partially) suppressed at the communication receiver. The higher the SINR at the communication receiver, the better the interference cancellation at the radar receiver.

Similarly, the higher the SINR at the radar receiver, the better the interference cancellation at the communication receiver.

In order to introduce interference cancellation, we consider the scenario where the communication signal arising from the closest smart traffic light is the only communication signal which is decoded. Therefore, the interference arising from the opposite lane is not cancelled, but the cooperation of both functions enables to mitigate the impact of S_R on the communication function, and S_C on the radar function. In that case, denoting by $\zeta_R(S_R, S_C) \equiv \zeta_R$ and $\zeta_C(S_R, S_C) \equiv \zeta_C$ the residual interference after interference cancellation, the metrics presented in Sections III-E to III-I are respectively rewritten as

$$\mathcal{P}_C^{\text{IC}}(\theta) = \mathbb{P}\left(\frac{S_C}{\zeta_R + I} \geq \theta\right), \quad (61)$$

$$\mathcal{P}_{\text{FA}}^{\text{IC}}(\gamma) = \mathbb{P}_{S_C, I}(\zeta_C + I \geq \gamma), \quad (62)$$

$$\mathcal{P}_D^{\text{IC}}(\gamma) = \mathbb{P}(S_R \kappa + \zeta_C + I \geq \gamma), \quad (63)$$

$$\mathcal{P}_S^{\text{IC}}(\theta') = \mathbb{P}\left(\frac{S_R \kappa}{\zeta_C + I} \geq \theta'\right), \quad (64)$$

$$\mathcal{D}^{\text{IC}}(\theta; \gamma) = \mathbb{P}\left(S_R \kappa + \zeta_C + I \geq \gamma, \frac{S_C}{\zeta_R + I} \geq \theta\right) \quad (65)$$

for a given $\mathcal{P}_{\text{FA}}^{\text{IC}}(\gamma)$,

$$S^{\text{IC}}(\theta', \theta) = \mathbb{P}\left(\frac{S_R \kappa}{\zeta_C + I} \geq \theta', \frac{S_C}{\zeta_R + I} \geq \theta\right). \quad (66)$$

The residual interference ζ_R is supposed to be high when the radar SIR is low since the radar receiver has difficulties to estimate correctly the delay and Doppler frequencies of the different targets. When this SIR is close to 0dB, the interference level could even be increased. Similarly, the same applies for ζ_C when the communication SIR is low since the communication receiver has difficulties to decode the communication signal and to estimate the associated parameters. Conversely, when these ratios are high, the interference is efficiently cancelled, leading to nearly zero residuals. For tractability, even if the total interference should be considered to assess the performance achieved by the interference cancellation, we assume that these functions do not depend on the aggregate interference I .

In this paper, three different cases are evaluated.

- 1) No interference cancellation is performed:

$$\zeta_R(S_R, S_C) = S_R, \quad \zeta_C(S_R, S_C) = S_C,$$

leading back to definitions given in Section III.

- 2) An imperfect interference cancellation is performed at both functions simultaneously, leading to the following residuals:

$$\zeta_R(S_R, S_C) = S_R \zeta\left(\frac{S_R}{S_C}\right),$$

$$\zeta_C(S_R, S_C) = S_C \zeta\left(\frac{S_C}{S_R}\right),$$

with

$$\zeta(x) = \frac{a}{1 + x^b}.$$

This function is illustrated in Figure 7 for different values of a and b . It has been designed to integrate the

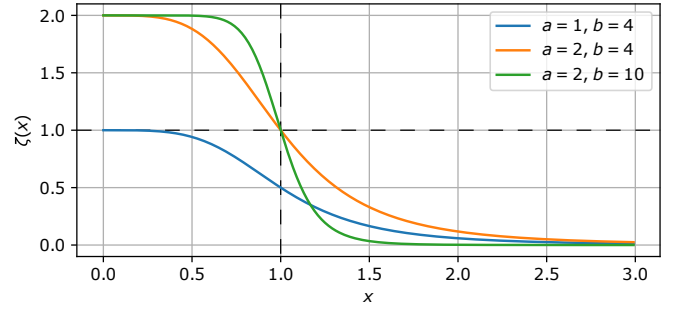


Fig. 7. Function ζ for different parameters.

positive and negative impacts of interference cancellation depending on the power levels S_R and S_C . Choosing $a > 1$ takes into account an increase of the interference for low power ratios.

- 3) A perfect interference cancellation is performed at both functions simultaneously, leading to null residuals:

$$\zeta_R(S_R, S_C) = 0 \quad \text{and/or} \quad \zeta_C(S_R, S_C) = 0$$

depending on whether the interference cancellation is performed at the radar receiver, at the communication receiver or at both functions.

Propositions 7 to 12 extend the results of Section III to integrate interference cancellation in the metrics.

Proposition 7: For a given communication SIR threshold θ , the coverage probability with interference cancellation is obtained as

$$\mathcal{P}_C^{\text{IC}}(\theta) = \mathcal{E}^{\Xi_C^{\text{IC}}} \left[\frac{1}{2} - \frac{1}{\pi} \int_0^\infty \frac{1}{\tau} \text{Im} \{ \mathcal{L}_I(-j\tau) \xi_C^{\text{IC}}(\tau) \} d\tau \right] \quad (67)$$

where

$$\xi_C^{\text{IC}}(\tau) = \exp \left(-j\tau \left(\frac{S_C}{\theta} - \zeta_R \right) \right) \quad (68)$$

and the area Ξ_C^{IC} is defined as

$$\Xi_C^{\text{IC}} \triangleq \left\{ \begin{array}{l} S_C - \theta \zeta_R \geq 0 \\ S_{R\min} \leq S_R \leq S_{R\max} \\ 0 \leq S_C \leq S_{C\max} \end{array} \right\}. \quad (69)$$

Proof: The proof is detailed in Appendix F-B. ■

Proposition 8: For a given threshold γ , the false alarm probability with interference cancellation is given by

$$\mathcal{P}_{\text{FA}}^{\text{IC}}(\gamma) = 1 - \mathcal{E}^{\Xi_F^{\text{IC}}} \left[\frac{1}{2} - \frac{1}{\pi} \int_0^\infty \frac{1}{\tau} \text{Im} \{ \mathcal{L}_I(-j\tau) \xi_F^{\text{IC}}(\tau) \} d\tau \right] \quad (70)$$

where

$$\xi_F^{\text{IC}}(\tau) = \exp(-j\tau(\gamma - \zeta_C)), \quad (71)$$

and the area Ξ_F^{IC} is defined as

$$\Xi_F^{IC} \triangleq \left\{ \begin{array}{l} \zeta_C \leq \gamma \\ S_{Rmin} \leq S_R \leq S_{Rmax} \\ 0 \leq S_C \leq S_{Cmax} \end{array} \right\}. \quad (72)$$

Proof: The proof is detailed in Appendix E-C. ■

Proposition 9: For a given threshold γ , the detection probability with interference cancellation is given by

$$\mathcal{P}_D^{IC}(\gamma) = 1 - \mathcal{E}^{\Xi_D^{IC}} \left[\frac{1}{2} - \frac{1}{\pi} \int_0^\infty \frac{1}{\tau} \text{Im} \{ \mathcal{L}_I(-j\tau) \xi_D^{IC}(\tau) \} d\tau \right] \quad (73)$$

where

$$\xi_D^{IC}(\tau) = \exp(-j\tau(\gamma - S_R\kappa - \zeta_C)), \quad (74)$$

and the area Ξ_D^{IC} is defined as

$$\Xi_D^{IC} \triangleq \left\{ \begin{array}{l} \gamma - S_R\kappa - \zeta_C \geq 0 \\ S_{Rmin} \leq S_R \leq S_{Rmax} \\ 0 \leq S_C \leq S_{Cmax} \end{array} \right\}. \quad (75)$$

Proof: The proof is detailed in Appendix E-B. ■

Proposition 10: For a given radar SIR threshold θ' , the success probability with interference cancellation is obtained as

$$\mathcal{P}_S^{IC}(\theta') = \mathcal{E}^{\Xi_S^{IC}} \left[\frac{1}{2} - \frac{1}{\pi} \int_0^\infty \frac{1}{\tau} \text{Im} \{ \mathcal{L}_I(-j\tau) \xi_S^{IC}(\tau) \} d\tau \right] \quad (76)$$

where

$$\xi_S^{IC}(\tau) = \exp \left(-j\tau \left(\frac{S_R\kappa}{\theta'} - \zeta_C \right) \right), \quad (77)$$

and the area Ξ_S^{IC} is defined as

$$\Xi_S^{IC} \triangleq \left\{ \begin{array}{l} \zeta_C \leq S_R\kappa/\theta' \\ S_{Rmin} \leq S_R \leq S_{Rmax} \\ 0 \leq S_C \leq S_{Cmax} \end{array} \right\}. \quad (78)$$

Proof: The proof is detailed in Appendix F-C. ■

Proposition 11: For a given false alarm probability \mathcal{P}_{FA} (and therefore for a given threshold γ) and a given communication SIR threshold θ , the JRDCCP metric with interference cancellation is obtained as

$$\begin{aligned} \mathcal{D}^{IC}(\theta; \gamma) = & -\mathcal{E}^{\Omega_{D2}^{IC}} \left[\frac{1}{\pi} \int_0^\infty \frac{1}{\tau} \text{Im} \{ \mathcal{L}_I(-j\tau) \psi_{D2}^{IC}(\tau) \} d\tau \right] \\ & + \mathcal{E}^{\Omega_{D1}^{IC}} \left[\frac{1}{2} - \frac{1}{\pi} \int_0^\infty \frac{1}{\tau} \text{Im} \{ \mathcal{L}_I(-j\tau) \psi_{D1}^{IC}(\tau) \} d\tau \right], \end{aligned} \quad (79)$$

where

$$\psi_{D1}^{IC}(\tau) = \xi_C^{IC}(\tau), \quad \psi_{D2}^{IC}(\tau) = \xi_C^{IC}(\tau) - \xi_D^{IC}(\tau), \quad (80)$$

and the areas Ω_{D1}^{IC} and Ω_{D2}^{IC} are defined as

$$\Omega_{D1}^{IC} \triangleq \left\{ \begin{array}{l} \gamma - S_R\kappa - \zeta_C \leq 0 \\ \frac{S_C}{\theta} - \zeta_R \geq 0 \\ S_{Rmin} \leq S_R \leq S_{Rmax} \\ 0 \leq S_C \leq S_{Cmax} \end{array} \right\}, \quad (81)$$

$$\Omega_{D2}^{IC} \triangleq \left\{ \begin{array}{l} \gamma - S_R\kappa - \zeta_C \geq 0 \\ \frac{S_C}{\theta} - \zeta_R \geq \gamma - S_R\kappa - \zeta_C \\ S_{Rmin} \leq S_R \leq S_{Rmax} \\ 0 \leq S_C \leq S_{Cmax} \end{array} \right\}. \quad (82)$$

Proof: The proof is detailed in Appendix E-A. ■

Proposition 12: For a given radar SIR threshold θ' and communication SIR threshold θ , the JRSCCP metric with interference cancellation is obtained as

$$\begin{aligned} \mathcal{S}^{IC}(\theta', \theta) = & \mathcal{E}^{\Omega_{S1}^{IC}} \left[\frac{1}{2} - \frac{1}{\pi} \int_0^\infty \frac{1}{\tau} \text{Im} \{ \mathcal{L}_I(-j\tau) \psi_{S1}^{IC}(\tau) \} d\tau \right] \\ & + \mathcal{E}^{\Omega_{S2}^{IC}} \left[\frac{1}{2} - \frac{1}{\pi} \int_0^\infty \frac{1}{\tau} \text{Im} \{ \mathcal{L}_I(-j\tau) \psi_{S2}^{IC}(\tau) \} d\tau \right], \end{aligned} \quad (83)$$

where

$$\psi_{S1}^{IC}(\tau) = \xi_S^{IC}(\tau), \quad \psi_{S2}^{IC}(\tau) = \xi_C^{IC}(\tau), \quad (84)$$

and the areas Ω_{S1}^{IC} and Ω_{S2}^{IC} are defined as

$$\Omega_{S1}^{IC} \triangleq \left\{ \begin{array}{l} \frac{S_R\kappa}{\theta'} - \zeta_C \geq 0 \\ \frac{S_C}{\theta} - \zeta_R \geq \frac{S_R\kappa}{\theta'} - \zeta_C \\ S_{Rmin} \leq S_R \leq S_{Rmax} \\ 0 \leq S_C \leq S_{Cmax} \end{array} \right\}, \quad (85)$$

$$\Omega_{S2}^{IC} \triangleq \left\{ \begin{array}{l} \frac{S_C}{\theta} - \zeta_R \geq 0 \\ \frac{S_R\kappa}{\theta'} - \zeta_C \geq \frac{S_C}{\theta} - \zeta_R \\ S_{Rmin} \leq S_R \leq S_{Rmax} \\ 0 \leq S_C \leq S_{Cmax} \end{array} \right\}. \quad (86)$$

Proof: The proof is detailed in Appendix F-A. ■

The upper and lower bounds are also generalised for the joint metrics with interference cancellation in Corollaries ?? using Fréchet inequalities.

Corollary 3: For a given false alarm probability \mathcal{P}_{FA}^{IC} with interference cancellation (and therefore for a given threshold γ) and a given communication SIR threshold θ , the JRDCCP metric with interference cancellation is bounded by

$$\mathcal{D}_m^{IC}(\theta; \gamma) \leq \mathcal{D}^{IC}(\theta; \gamma) \leq \mathcal{D}_M^{IC}(\theta; \gamma), \quad (87)$$

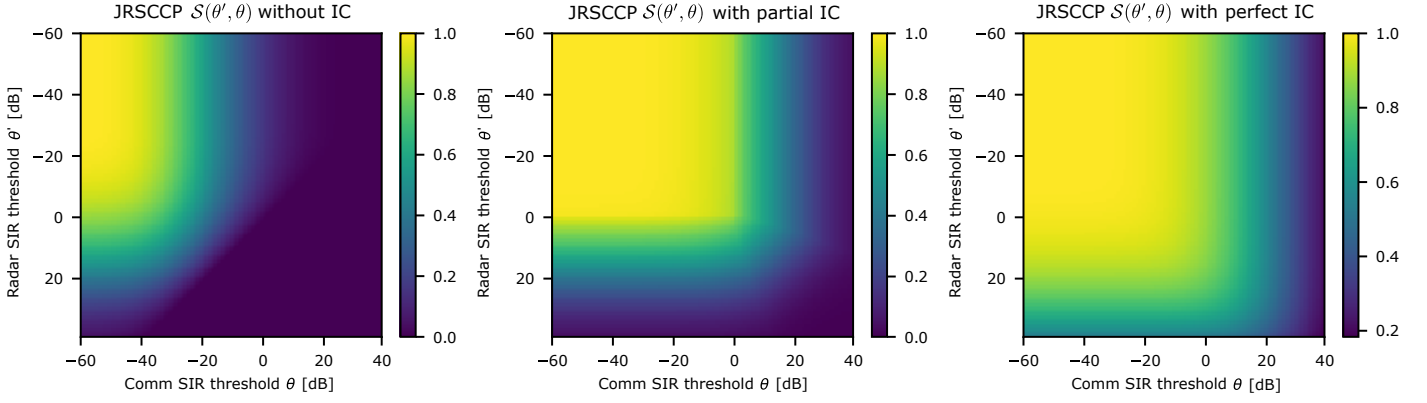


Fig. 8. JRSCCP metric with different interference cancellation schemes.

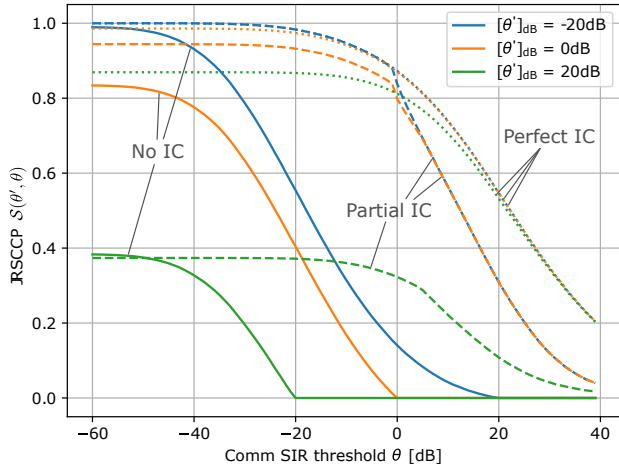


Fig. 9. JRSCCP metric with different interference cancellation schemes, for $\theta' = \{-20, 0, 20\}$ dB.

with

$$\mathcal{D}_m^{\text{IC}}(\theta; \gamma) = \max(0, \mathcal{P}_D^{\text{IC}}(\gamma) + \mathcal{P}_C^{\text{IC}}(\theta) - 1), \quad (88)$$

$$\mathcal{D}_m^{\text{IC}}(\theta; \gamma) = \min(\mathcal{P}_D^{\text{IC}}(\gamma), \mathcal{P}_C^{\text{IC}}(\theta)). \quad (89)$$

Similarly, for a given radar SIR threshold θ' and communication SIR threshold θ , the JRSCCP metric is bounded by

$$\mathcal{S}_m^{\text{IC}}(\theta', \theta) \leq \mathcal{S}^{\text{IC}}(\theta', \theta) \leq \mathcal{S}_M^{\text{IC}}(\theta', \theta), \quad (90)$$

with

$$\mathcal{S}_m^{\text{IC}}(\theta', \theta) = \max(0, \mathcal{P}_S^{\text{IC}}(\theta') + \mathcal{P}_C^{\text{IC}}(\theta) - 1), \quad (91)$$

$$\mathcal{S}_M^{\text{IC}}(\theta', \theta) = \min(\mathcal{P}_S^{\text{IC}}(\theta'), \mathcal{P}_C^{\text{IC}}(\theta)). \quad (92)$$

Proof: The proposed bounds are given by Fréchet inequalities.

Finally, the conditional metrics are rewritten as follows:

$$\mathcal{P}_{C|D}^{\text{IC}}(\theta; \gamma) = \mathbb{P}\left(\frac{S_C}{\zeta_R + I} \geq \theta \mid S_{R\kappa} + \zeta_C + I \geq \gamma\right) \quad (93)$$

for a given $\mathcal{P}_{FA}^{\text{IC}}(\gamma)$,

$$\mathcal{P}_{C|S}^{\text{IC}}(\theta; \theta') = \mathbb{P}\left(\frac{S_C}{\zeta_R + I} \geq \theta \mid \frac{S_{R\kappa}}{\zeta_C + I} \geq \theta'\right). \quad (94)$$

$$\mathcal{P}_{D|C}^{\text{IC}}(\gamma; \theta) = \mathbb{P}\left(S_{R\kappa} + \zeta_C + I \geq \gamma \mid \frac{S_C}{\zeta_R + I} \geq \theta\right) \quad (95)$$

for a given $\mathcal{P}_{FA}^{\text{IC}}(\gamma)$,

$$\mathcal{P}_{S|C}^{\text{IC}}(\theta'; \theta) = \mathbb{P}\left(\frac{S_{R\kappa}}{\zeta_C + I} \geq \theta' \mid \frac{S_C}{\zeta_R + I} \geq \theta\right). \quad (96)$$

Their expressions are given in Corollaries 4.

Corollary 4: For a given false alarm probability \mathcal{P}_{FA} (and therefore for a given threshold γ) or a given radar SIR threshold θ' , the coverage probabilities achieved by vehicles performing successfully the radar function with interference cancellation for a given communication SIR threshold θ are given by

$$\mathcal{P}_{C|D}^{\text{IC}}(\theta; \gamma) = \mathcal{D}^{\text{IC}}(\theta; \gamma) / \mathcal{P}_D^{\text{IC}}(\gamma) \quad (97)$$

and

$$\mathcal{P}_{C|S}^{\text{IC}}(\theta; \theta') = \mathcal{S}^{\text{IC}}(\theta', \theta) / \mathcal{P}_S^{\text{IC}}(\theta'). \quad (98)$$

Similarly, the detection and success probabilities achieved by vehicles performing successfully the communication function with interference cancellation are given by

$$\mathcal{P}_{D|C}^{\text{IC}}(\gamma; \theta) = \mathcal{D}^{\text{IC}}(\theta; \gamma) / \mathcal{P}_C^{\text{IC}}(\theta) \quad (99)$$

and

$$\mathcal{P}_{S|C}^{\text{IC}}(\theta'; \theta) = \mathcal{S}^{\text{IC}}(\theta', \theta) / \mathcal{P}_C^{\text{IC}}(\theta). \quad (100)$$

Proof: These results are obtained using Bayes law.

Figure 8 and 9 illustrates the impact of the different interference cancellation schemes on the JRSCCP metric: perfect

interference cancellation, partial interference cancellation with $a = 2$ and $b = 4$, or no interference cancellation at all. Note that with this choice of parameters, the residual interference ζ_R (resp. ζ_C) at the communication function (resp. radar function) is increased when the power ratio S_R/S_C (resp. S_C/S_R) is less than 0dB, as illustrated in Figure 7.

With perfect interference cancellation, the performance drastically increases since the interference power is in most cases lower than the radar and communication powers. With partial interference cancellation, the achieved performance depends on the considered radar and communication SIR threshold. At high radar (resp. communication) SIR thresholds, it is likely that the communication (resp. radar) signal is dominant for the metric to be non zero. In that situation, the interference cancellation performs well at the communication (resp. radar) function, but the interference level is potentially increased at the other function. However, in most cases, the achieved performance is improved thanks to partial interference cancellation.

VI. CONCLUSION

In this paper, a new automotive scenario with smart traffic lights and vehicles, both equipped with joint radar-communication systems, has been analysed. In order to analyse the performance of both functions separately or jointly, multiple metrics, upper and lower bounds have been developed using stochastic geometry. Based on that, optimisation of the powers of the vehicles and traffic lights has also been performed. Finally, the metrics have been extended to include a new model of interference cancellation at both functions.

In future works, other models and schemes for the interference cancellation could be considered, i.e. suppressing the interference at the radar or communication function only. Additionally, both metrics could be generalised for other joint radar-communication scenarios, for instance indoor communication and localisation. Finally, this work can be extended by comparing the developed metrics with these obtained through Monte-Carlo simulations with a complexified system model, and ray tracing simulations.

REFERENCES

- [1] L. Zheng, M. Lops, Y. C. Eldar, and X. Wang, "Radar and Communication Co-existence: an Overview," 2019.
- [2] F. Liu, C. Masouros, and S. Member, "A Tutorial on Joint Radar and Communication Transmission for Vehicular Networks - Part I : Background and Fundamentals," vol. 7798, no. c, pp. 3–7, 2020.
- [3] N. C. Luong, X. Lu, D. T. Hoang, D. Niyato, and D. I. Kim, "Radio Resource Management in Joint Radar and Communication: A Comprehensive Survey," *IEEE Communications Surveys and Tutorials*, vol. 23, no. 2, pp. 780–814, 2021.
- [4] F. Baccelli and B. Blaszczyzyn, *Stochastic Geometry and Wireless Networks: Volume I Theory*. 2010.
- [5] F. Baccelli and B. Blaszczyzyn, *Stochastic Geometry and Wireless Networks: Volume II Applications*. 2010.
- [6] M. Kafafy, A. S. Ibrahim, and M. H. Ismail, "Stochastic Geometry-Based Performance Analysis of Cellular Systems in the Vicinity of Rotating Radars," *IEEE Communications Letters*, vol. 25, no. 4, pp. 1391–1395, 2021.
- [7] M. Haenggi, J. Andrews, F. Baccelli, O. Dousse, and M. Franceschetti, "Guest editorial geometry and random graphs for the analysis and design of wireless networks," *IEEE Journal on Selected Areas in Communications*, vol. 27, no. 7, pp. 1025–1028, 2009.
- [8] Y. Hmamouche, M. Benjillali, S. Saoudi, H. Yanikomeroğlu, and M. D. Renzo, "New Trends in Stochastic Geometry for Wireless Networks: A Tutorial and Survey," *Proceedings of the IEEE*, vol. 109, no. 7, pp. 1200–1252, 2021.
- [9] S. Singh, X. Zhang, and J. G. Andrews, "Joint rate and sinr coverage analysis for decoupled uplink-downlink biased cell associations in het-nets," *IEEE Transactions on Wireless Communications*, vol. 14, no. 10, pp. 5360–5373, 2015.
- [10] M. Di Renzo and W. Lu, "System-level analysis and optimization of cellular networks with simultaneous wireless information and power transfer: Stochastic geometry modeling," *IEEE Transactions on Vehicular Technology*, vol. 66, no. 3, pp. 2251–2275, 2017.
- [11] A. Munari, L. Simic, and M. Petrova, "Stochastic geometry interference analysis of radar network performance," *IEEE Communications Letters*, vol. 22, no. 11, pp. 2362–2365, 2018.
- [12] S. S. Ram, G. Singh, and G. Ghatak, "Estimating radar detection coverage probability of targets in a cluttered environment using stochastic geometry," *2020 IEEE International Radar Conference, RADAR 2020*, pp. 665–670, 2020.
- [13] S. S. Ram, G. Singh, and G. Ghatak, "Optimization of Radar Parameters for Maximum Detection Probability Under Generalized Discrete Clutter Conditions Using Stochastic Geometry," *IEEE Open Journal of Signal Processing*, vol. 2, pp. 571–585, 2021.
- [14] S. S. Ram and G. Ghatak, "Estimation of Bistatic Radar Detection Performance Under Discrete Clutter Conditions Using Stochastic Geometry," pp. 1–16, 2022.
- [15] J. Park and R. W. H. Jr, "Analysis of Blockage Sensing by RADARs in Random Cellular Networks," *IEEE Signal Processing Letters*, vol. 25, no. 11, pp. 1620–1624, 2018.
- [16] P. Ren, A. Munari, and M. Petrova, "Performance tradeoffs of joint radar-communication networks," *IEEE Wireless Communications Letters*, vol. 8, no. 1, pp. 165–168, 2019.
- [17] P. Ren, A. Munari, and M. Petrova, "Performance Analysis of a Time-sharing Joint Radar-Communications Network," pp. 908–913, 2021.
- [18] M. Kafafy, A. S. Ibrahim, and M. H. Ismail, "Stochastic Geometry-Based Performance Analysis of Cellular Systems in the Vicinity of Rotating Radars," *IEEE Communications Letters*, vol. 25, no. 4, pp. 1391–1395, 2021.
- [19] R. M. Rao, H. S. Dhillon, V. Marojevic, and J. H. Reed, "Underlay radar-massive MIMO spectrum sharing: Modeling fundamentals and performance analysis," *IEEE Transactions on Wireless Communications*, vol. 20, no. 11, pp. 7213–7229, 2021.
- [20] C. Skouroumounis, C. Psomas, and I. Krikidis, "Cooperative detection for mmwave radar-communication systems," *2020 IEEE International Conference on Communications Workshops, ICC Workshops 2020 - Proceedings*, 2020.
- [21] C. Skouroumounis, C. Psomas, and I. Krikidis, "FD-JCAS Techniques for mmWave HetNets: Ginibre Point Process Modeling and Analysis," *IEEE Transactions on Mobile Computing*, vol. 1233, no. c, pp. 1–15, 2021.
- [22] Z. Fang, Z. Wei, Z. Feng, X. Chen, and Z. Guo, "Performance of joint radar and communication enabled cooperative detection," *2019 IEEE/CIC International Conference on Communications in China, ICCIC 2019*, no. Iccic, pp. 753–758, 2019.
- [23] S. S. Ram and G. Ghatak, "Optimization of Network Throughput of Joint Radar Communication System Using Stochastic Geometry," pp. 1–23, 2022.
- [24] Z. Fang, Z. Wei, X. Chen, H. Wu, and Z. Feng, "Stochastic geometry for automotive radar interference with RCS characteristics," *IEEE Wireless Communications Letters*, vol. 9, no. 11, pp. 1817–1820, 2020.
- [25] A. Al-Hourani, R. J. Evans, S. Kandeepan, B. Moran, and H. Eltom, "Stochastic Geometry Methods for Modeling Automotive Radar Interference," *IEEE Transactions on Intelligent Transportation Systems*, vol. 19, no. 2, pp. 333–344, 2018.
- [26] K. V. Mishra, B. Shankar M. R., and B. Ottersten, "Stochastic-Geometry-Based Interference Modeling in Automotive Radars Using Matérn Hard-Core Process," *IEEE National Radar Conference - Proceedings*, vol. 2020-Sept, 2020.
- [27] Z. Fang, Z. Wei, H. Ma, X. Chen, and Z. Feng, "Analysis of Automotive Radar Interference among Multiple Vehicles," *2020 IEEE Wireless*

- [28] P. Chu, J. A. Zhang, X. Wang, Z. Fei, G. Fang, and D. Wang, "Interference Characterization and Power Optimization for Automotive Radar with Directional Antenna," *IEEE Transactions on Vehicular Technology*, vol. 69, no. 4, pp. 3703–3716, 2020.
- [29] G. Ghatak, S. S. Kalamkar, Y. Gupta, and S. Sharma, "A Fine-Grained Analysis of Radar Detection in Vehicular Networks," vol. 9545, no. c, pp. 01–06, 2022.
- [30] G. Ghatak, S. Kalamkar, and Y. Gupta, "Radar detection in vehicular networks: Fine-grained analysis and optimal channel access," *IEEE Transactions on Vehicular Technology*, pp. 1–1, 2022.
- [31] H. Ma, Z. Wei, X. Chen, Z. Fang, Y. Liu, F. Ning, and Z. Feng, "Performance analysis of joint radar and communication enabled vehicular ad hoc network," *2019 IEEE/CIC International Conference on Communications in China, ICCIC 2019*, no. Iccic, pp. 887–892, 2019.
- [32] D. Ghazlani, A. Omri, S. Bouallegue, H. Chamkhia, and R. Bouallegue, "Stochastic Geometry-based Analysis of Joint Radar and Communication-Enabled Cooperative Detection Systems," pp. 325–330, 2021.
- [33] H. Friis, "A note on a simple transmission formula," *Proceedings of the IRE*, vol. 34, no. 5, pp. 254–256, 1946.
- [34] M. A. Richards, *Fundamentals of Radar Signal Processing*. McGraw-Hill Professional, 2005.
- [35] J. Gil-Pelaez, "Note on the inversion theorem," *Biometrika*, vol. 38, pp. 481–482, 12 1951.
- [36] M. Fréchet, "Généralisation du théorème des probabilités totales," *Fundamenta Mathematicae*, vol. 25, no. 1, pp. 379–387, 1935.

APPENDIX A

PROBABILITY DENSITY FUNCTIONS OF r_R AND r_C

Let us denote by $\Psi_{\Phi_R}(A)$ the random counting measure of Φ_R on the subset A . Knowing that the void probability of a PPP of density λ is given by

$$\mathbb{P}_{\Psi_{\Phi}}(\Psi_{\Phi}(A) = 0) = \exp\left(-\int_A \lambda(\mathbf{x})d\mathbf{x}\right),$$

The probability to have at least one vehicle in the radar detectable range is given by

$$\begin{aligned}\mathbb{P}_{\Psi_{\Phi_R}}(\Psi_{\Phi_R}([r_{Rmin}, r_{Rmax}]) > 0) \\ = 1 - \exp(-\lambda_V(r_{Rmax} - r_{Rmin})).\end{aligned}$$

Knowing that, thanks to the Bayes rule, the complementary CDF of r_R assuming that there is at least one vehicle in the radar detection range can be developed as

$$\begin{aligned}\bar{F}_{r_R}(r) &= \mathbb{P}_{r_R, \Psi_{\Phi_R}}(r_R > r \mid \Psi_{\Phi_R}([r_{Rmin}, r_{Rmax}]) > 0) \\ &= \frac{\mathbb{P}_{r_R, \Psi_{\Phi_R}}(\Psi_{\Phi_R}([0, r]) = 0, \Psi_{\Phi_R}([r_{Rmin}, r_{Rmax}]) > 0)}{\mathbb{P}_{\Psi_{\Phi_R}}(\Psi_{\Phi_R}([r_{Rmin}, r_{Rmax}]) > 0)}.\end{aligned}$$

Three cases can be distinguished:

- 1) When $r \leq r_{Rmin}$, the two subsets $[0, r]$ and $[r_{Rmin}, r_{Rmax}]$ are disjoint, and therefore, from the properties of PPPs, the counting measures evaluated on these two subsets are independent. Thus,

$$\bar{F}_{r_R}(r) = \mathbb{P}_{r_R, \Psi_{\Phi_R}}(\Psi_{\Phi_R}([0, r]) = 0) = 1.$$

- 2) When $r_{Rmax} \leq r$, $[r_{Rmin}, r_{Rmax}]$ is a subset of $[0, r]$, and therefore $\bar{F}_{r_R}(r) = 0$.

- 3) When $r_{Rmin} \leq r \leq r_{Rmax}$, based on the void probability of PPPs, the numerator of the above expression can be developed as

$$\begin{aligned}\mathbb{P}_{r_R, \Psi_{\Phi_R}}(\Psi_{\Phi_R}([0, r]) = 0, \Psi_{\Phi_R}([r_{Rmin}, r_{Rmax}]) > 0) \\ = \mathbb{P}_{r_R, \Psi_{\Phi_R}}(\Psi_{\Phi_R}([r_{Rmin}, r]) = 0, \Psi_{\Phi_R}([r, r_{Rmax}]) > 0) \\ = \exp(-\lambda_V(r - r_{Rmin}))[1 - \exp(-\lambda_V(r_{Rmax} - r))].\end{aligned}$$

Finally the PDF of r_R is obtained by derivating the opposite of the cumulative CDF, and 1 is obtained. Equation (7) can be demonstrated similarly.

APPENDIX B

PROBABILITY DENSITY FUNCTIONS OF S_R AND S_C

These results directly follow from the change of variable of an univariate PDF with a monotonic and invertible function: let $g : A \in \mathbb{R} \rightarrow B \in \mathbb{R}$ be a monotonic and invertible function and $Y = g(X)$ with X and Y two random variables, the PDF of Y is obtained as

$$f_Y(y) = f_X(g^{-1}(y)) \left| \frac{d}{dy} g^{-1}(y) \right|,$$

where $f_X(x)$ is the PDF of X and g^{-1} denotes the inverse function of g . For the radar link, (5) is inverted as $r_R(s) = \rho_R^{\frac{1}{\alpha_R}} s^{-\frac{1}{\alpha_R}}$, and

$$\left| \frac{d}{ds} r_R(s) \right| = \frac{\rho_R^{\frac{1}{\alpha_R}} s^{-\frac{1}{\alpha_R}-1}}{\alpha_R} = \frac{r_R(s)}{\alpha_R s},$$

leading to (8). For the communication link, (2) is inverted as

$$r_C(s) = \sqrt{\rho_C^{\frac{2}{\alpha_C}} s^{-\frac{2}{\alpha_C}} - d_C^2}, \text{ and}$$

$$\begin{aligned}\left| \frac{d}{ds} r_C(s) \right| &= \frac{2\rho_C^{\frac{2}{\alpha_C}} s^{-\frac{2}{\alpha_C}-1}}{\alpha_C} \frac{1}{2\sqrt{\rho_C^{\frac{2}{\alpha_C}} s^{-\frac{2}{\alpha_C}} - d_C^2}} \\ &= \frac{r_C^2(s) + d_C^2}{\alpha_C s r_C(s)},\end{aligned}$$

leading to (9).

APPENDIX C

LAPLACE TRANSFORM OF $|h_i|^2$

Let us denote by ν^2 the power of the dominant path and $2\sigma^2$ the power of the scattered paths of an interfering link. The small-scale fading is expressed in cartesian coordinates as $|h_i|^2 = X^2 + Y^2$ where $X \sim \mathcal{N}(\nu \cos \theta, \sigma^2)$ and $Y \sim \mathcal{N}(\nu \sin \theta, \sigma^2)$ are independent normally distributed random variables, with $\theta \in [0, 2\pi[$. By the properties of the normal distribution, it is known that X^2/σ^2 and Y^2/σ^2 follow chi-square distributions with one degree of freedom. Therefore we have

$$\mathcal{L}_{X^2}(s) = \exp\left(-\frac{\nu^2 \cos^2 \theta}{1 + 2\sigma^2 s}\right) (1 + 2\sigma^2 s)^{-\frac{1}{2}}$$

and

$$\mathcal{L}_{Y^2}(s) = \exp\left(-\frac{\nu^2 \sin^2 \theta}{1 + 2\sigma^2 s}\right) (1 + 2\sigma^2 s)^{-\frac{1}{2}}.$$

Finally, (10) is obtained knowing that $\mathcal{L}_{|h_i|^2}(s) = \mathcal{L}_{X^2}(s)\mathcal{L}_{Y^2}(s)$,

$$\nu^2 = \frac{K}{K+1} \Omega, \quad 2\sigma^2 = \frac{1}{K+1} \Omega,$$

and $\mathbb{E}[|h_i|^2] = \Omega = 1$ with a normalised power.

APPENDIX D LAPLACE TRANSFORM OF I

By developing the definition of the Laplace transform of I ,

$$\begin{aligned} \mathcal{L}_I(s) &= \mathbb{E} \left[\exp \left(-s \sum_{i | \phi_i \in \Phi_I} \rho_I (\|\phi_i\|^2 + d_I^2)^{-\frac{\alpha_I}{2}} |h_i|^2 \right) \right] \\ &\stackrel{(a)}{=} \mathbb{E}_{\Phi_I} \left[\prod_{i | \phi_i \in \Phi_I} \mathbb{E}_{h_i} \left[\exp \left(-s \rho_I (\|\phi_i\|^2 + d_I^2)^{-\frac{\alpha_I}{2}} |h_i|^2 \right) \right] \right] \\ &\stackrel{(b)}{=} \exp \left(-\lambda_I \int_{r_{I\min}}^{\infty} \left(1 - \mathcal{L}_{|h_i|^2} \left(s \rho_I (r^2 + d_I^2)^{-\frac{\alpha_I}{2}} \right) \right) dr \right) \end{aligned}$$

where (a) is obtained thanks to the independency of the small-scale fading of each interfering link, and (b) follows from the Probability Generating Functional of a PPP.

APPENDIX E JRDCCP AND DERIVED METRICS

A. JRDCCP metric

1) *With interference cancellation:* The JRDCCP metric can be developed as

$$\begin{aligned} \mathcal{D}^{\text{IC}}(\theta; \gamma) &= \mathbb{P}_{S_R, S_C, I} \left(S_R \kappa + \zeta_C + I \geq \gamma, \frac{S_C}{\zeta_R + I} \geq \theta \right) \\ &= \mathbb{E}_{S_R, S_C} \left[\mathbb{P}_{I | S_R, S_C} \left(\gamma - S_R \kappa - \zeta_C \leq I \leq \frac{S_C}{\theta} - \zeta_R \right) \right]. \end{aligned}$$

This probability is non zero either when

$$\begin{cases} \gamma - S_R \kappa - \zeta_C \leq 0 \\ \frac{S_C}{\theta} - \zeta_R \geq 0 \end{cases} \quad (101)$$

or when

$$\begin{cases} \gamma - S_R \kappa - \zeta_C \geq 0 \\ \frac{S_C}{\theta} - \zeta_R \geq \gamma - S_R \kappa - \zeta_C \end{cases}, \quad (102)$$

leading to the areas Ω_{D1}^{IC} and Ω_{D2}^{IC} given in (82) including the radar and communication power constraints.

In Ω_{D1}^{IC} , applying the Gil-Pelaez theorem,

$$\begin{aligned} \mathbb{P}_{I | S_R, S_C} \left(I \leq \frac{S_C}{\theta} - \zeta_R \right) &= \\ \frac{1}{2} - \frac{1}{\pi} \int_0^{\infty} \frac{1}{\tau} \text{Im} \{ \mathcal{L}_I(-j\tau) \psi_{D1}^{\text{IC}}(\tau) \} d\tau \end{aligned}$$

with ψ_{D1}^{IC} given in (80).

In Ω_{D2}^{IC} , applying the Gil-Pelaez theorem,

$$\begin{aligned} \mathbb{P}_{I | S_R, S_C} \left(\gamma - S_R \kappa - \zeta_C \leq I \leq \frac{S_C}{\theta} - \zeta_R \right) &= \\ \mathbb{P}_{I | S_R, S_C} \left(I \leq \frac{S_C}{\theta} - \zeta_R \right) &- \mathbb{P}_{I | S_R, S_C} (I \leq \gamma - S_R \kappa - \zeta_C) \\ = -\frac{1}{\pi} \int_0^{\infty} \frac{1}{\tau} \text{Im} \{ \mathcal{L}_I(-j\tau) \psi_{D2}^{\text{IC}}(\tau) \} d\tau \end{aligned}$$

with ψ_{D2}^{IC} given in (80), leading finally to (79).

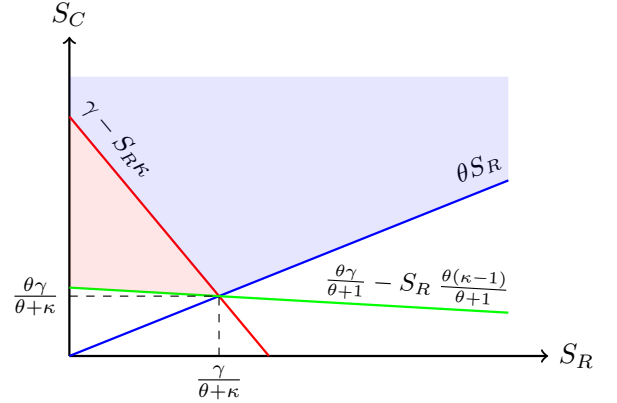
2) *Without interference cancellation:* Without interference cancellation, (101) and (102) are respectively rewritten as

$$\begin{cases} \gamma - S_R \kappa - S_C \leq 0 \\ \frac{S_C}{\theta} - S_R \geq 0 \end{cases} \Leftrightarrow S_C \geq \max(\theta S_R, \gamma - S_R \kappa),$$

and

$$\begin{cases} \gamma - S_R \kappa - S_C \geq 0 \\ \frac{S_C}{\theta} - S_R \geq \gamma - S_R \kappa - S_C \end{cases} \Leftrightarrow \frac{\theta \gamma}{\theta + 1} - S_R \frac{\theta(\kappa - 1)}{\theta + 1} \leq S_C \leq \gamma - \kappa S_R.$$

These conditions respectively lead to the blue and red areas on this plot (note that $S_{R\min}$, $S_{R\max}$ and $S_{C\max}$ are not illustrated):



and the areas Ω_{D1}^{IC} and Ω_{D2}^{IC} are then respectively rewritten as Ω_{D1} and Ω_{D2} given in (39). Finally, the functions ψ_{D1}^{IC} and ψ_{D2}^{IC} of (80) are replaced by ψ_{D1} and ψ_{D2} given in (37), leading to (36).

B. Detection probability

1) *With interference cancellation:* The detection probability is obtained as

$$\mathcal{P}_D^{\text{IC}}(\gamma) = \lim_{\theta \rightarrow 0} \mathcal{D}^{\text{IC}}(\theta; \gamma).$$

In that case, the area Ω_{D2}^{IC} is restricted to Ξ_D^{IC} given in (28), and the area Ω_{D1}^{IC} is restricted to $\Xi_D^{\text{IC}^c}$, where \cdot^c denotes the complement set. In $\Xi_D^{\text{IC}^c}$, we have

$$\lim_{\theta \rightarrow 0} \mathbb{P}_{I | S_R, S_C} \left(I \leq \frac{S_C}{\theta} - \zeta_R \right) = 1.$$

In Ξ_D^{IC} , we have

$$\begin{aligned} & \lim_{\theta \rightarrow 0} \mathbb{P}_{I|S_R, S_C} \left(\gamma - S_R \kappa - \zeta_C \leq I \leq \frac{S_C}{\theta} - \zeta_R \right) \\ &= \mathbb{P}_{I|S_R, S_C} (I \geq \gamma - S_R \kappa - \zeta_C) \\ &= \frac{1}{2} + \frac{1}{\pi} \int_0^\infty \frac{1}{\tau} \text{Im} \{ \mathcal{L}_I(-j\tau) \xi_D^{\text{IC}}(\tau) \} d\tau \end{aligned}$$

with ξ_D^{IC} given in (74).

Finally, (73) is obtained knowing that

$$\mathcal{E}^{\Xi_D^{\text{IC}}} [1] = 1 - \mathcal{E}^{\Xi_D^{\text{IC}}} [1].$$

2) *Without interference cancellation:* Without interference cancellation, ξ_D^{IC} and Ξ_D^{IC} are rewritten as ξ_D and Ξ_D given in (27) and (28).

C. False alarm probability

1) *With interference cancellation:* The false alarm probability with interference cancellation is identical to the detection probability with interference cancellation, except that the radar echo is suppressed from the received power. In that case, ξ_D^{IC} and Ξ_D^{IC} are replaced by ξ_F^{IC} and Ξ_F^{IC} given in (71) and (72).

2) *Without interference cancellation:* Without interference cancellation, ξ_D^{IC} and Ξ_D^{IC} are rewritten as ξ_F and Ξ_F given in (24) and (25).

APPENDIX F JRSCCP AND DERIVED METRICS

A. JRSCCP metric

1) *With interference cancellation:* The JRSCCP metric with interference cancellation can be developed as

$$\begin{aligned} \mathcal{S}(\theta', \theta) &= \mathbb{P}_{S_R, S_C, I} \left(\frac{S_R \kappa}{S_C + I} \geq \theta', \frac{S_C}{S_R + I} \geq \theta \right) \\ &= \mathbb{E}_{S_R, S_C} \left[\mathbb{P}_{I|S_R, S_C} \left(I \leq \frac{S_R \kappa}{\theta'} - \zeta_C, I \leq \frac{S_C}{\theta} - \zeta_R \right) \right]. \end{aligned}$$

This probability is non zero either if

$$\begin{cases} \frac{S_R \kappa}{\theta'} - \zeta_C \geq 0 \\ \frac{S_C}{\theta} - \zeta_R \geq \frac{S_R \kappa}{\theta'} - \zeta_C \end{cases}, \quad (103)$$

or

$$\begin{cases} \frac{S_C}{\theta} - \zeta_R \geq 0 \\ \frac{S_R \kappa}{\theta'} - \zeta_C \geq \frac{S_C}{\theta} - \zeta_R \end{cases}, \quad (104)$$

leading to the areas Ω_{S1}^{IC} and Ω_{S2}^{IC} given in (86) including the radar and communication power constraints.

In Ω_{S1}^{IC} , applying the Gil-Pelaez theorem,

$$\begin{aligned} & \mathbb{P}_{I|S_R, S_C} \left(I \leq \frac{S_R \kappa}{\theta'} - \zeta_C, I \leq \frac{S_C}{\theta} - \zeta_R \right) \\ &= \mathbb{P}_{I|S_R, S_C} \left(I \leq \frac{S_R \kappa}{\theta'} - \zeta_C \right) \\ &= \frac{1}{2} - \frac{1}{\pi} \int_0^\infty \frac{1}{\tau} \text{Im} \{ \mathcal{L}_I(-j\tau) \psi_{S1}^{\text{IC}}(\tau) \} d\tau \end{aligned}$$

with ψ_{S1}^{IC} given in (84).

In Ω_{S2}^{IC} , applying the Gil-Pelaez theorem,

$$\begin{aligned} & \mathbb{P}_{I|S_R, S_C} \left(I \leq \frac{S_R \kappa}{\theta'} - \zeta_C, I \leq \frac{S_C}{\theta} - \zeta_R \right) \\ &= \mathbb{P}_{I|S_R, S_C} \left(I \leq \frac{S_C}{\theta} - \zeta_R \right) \\ &= \frac{1}{2} - \frac{1}{\pi} \int_0^\infty \frac{1}{\tau} \text{Im} \{ \mathcal{L}_I(-j\tau) \psi_{S2}^{\text{IC}}(\tau) \} d\tau \end{aligned}$$

with ψ_{S2}^{IC} given in (84), leading finally to (83).

2) *Without interference cancellation:* Without interference cancellation, the JRSCCP is non zero only if

$$\begin{cases} \frac{S_R \kappa}{\theta'} - S_C \geq 0 \\ \frac{S_C}{\theta} - S_R \geq 0 \end{cases} \Leftrightarrow \theta S_R \leq S_C \leq \frac{S_R \kappa}{\theta'},$$

which is fulfilled only if

$$\theta \theta' \leq \kappa \Leftrightarrow [\theta]_{\text{dB}} + [\theta']_{\text{dB}} \leq [\kappa]_{\text{dB}}.$$

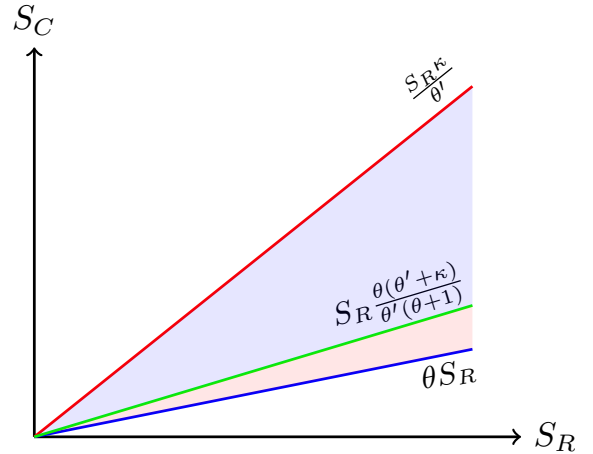
Then, (103) and (104) are respectively rewritten as

$$\begin{cases} \frac{S_R \kappa}{\theta'} - S_C \geq 0 \\ \frac{S_C}{\theta} - S_R \geq \frac{S_R \kappa}{\theta'} - S_C \end{cases} \Leftrightarrow S_R \frac{\theta(\theta' + \kappa)}{\theta'(\theta + 1)} \leq S_C \leq \frac{S_R \kappa}{\theta'},$$

and

$$\begin{cases} \frac{S_C}{\theta} - S_R \geq 0 \\ \frac{S_R \kappa}{\theta'} - S_C \geq \frac{S_C}{\theta} - S_R \end{cases} \Leftrightarrow \theta S_R \leq S_C \leq S_R \frac{\theta(\theta' + \kappa)}{\theta'(\theta + 1)}.$$

These two cases respectively lead to the blue and red areas on this plot (note that $S_{R\min}$, $S_{R\max}$ and $S_{C\max}$ are not illustrated):



The areas Ω_{S1}^{IC} and Ω_{S2}^{IC} are then respectively rewritten as Ω_{S1} and Ω_{S2} given in (45). Finally, the functions ψ_{S1}^{IC} and ψ_{S2}^{IC} of (84) are respectively rewritten as ψ_{S1} and ψ_{S2} given in (43), leading to (42).

B. Coverage probability

1) *With interference cancellation:* The coverage probability is obtained as

$$\mathcal{P}_C^{\text{IC}}(\theta) = \lim_{\theta' \rightarrow 0} \mathcal{S}^{\text{IC}}(\theta', \theta).$$

In that case, Ω_{S1}^{IC} vanishes and Ω_{S2}^{IC} becomes Ξ_C^{IC} given in (69), leading to (67).

2) *Without interference cancellation:* Without interference cancellation, ψ_{S2}^{IC} and Ξ_C^{IC} are respectively rewritten as ξ_C and Ξ_C given in (14) and (15).

C. Success probability

1) *With interference cancellation:* The success probability is obtained as

$$\mathcal{P}_S^{\text{IC}}(\theta') = \lim_{\theta \rightarrow 0} \mathcal{S}^{\text{IC}}(\theta', \theta).$$

In that case, Ω_{S2}^{IC} vanishes and Ω_{S1}^{IC} becomes Ξ_C^{IC} given in (69).

2) *Without interference cancellation:* Without interference cancellation, ψ_{S1}^{IC} and Ξ_S^{IC} are respectively rewritten as ξ_S and Ξ_S given in (33) and (34).